*Optica Applicata, Vol. XX, No. 2, 1990*

# Thermal properties of p-side-down ridge-waveguide lasers. I. Theoretical model

W. NAKWASKI

Institute of Physics, Technical University of Łódź, ul. Wólczańska 219, 93-005 Łódź, Poland.

W. BOTH

Optoelectronics Division, Central Institute of Optics and Spectroscopy, Rudower Chaussee 6, Berlin–1199, GDR.

A thermal model of a p-side-down configuration of a ridge-waveguide (RW) laser diode is presented in this work. In the model, the multilayer structure of the laser, the thermal resistance of contact layers, the spreading thermal resistance of a heat sink and the radiative transfer of the spontaneous emission are taken into account. The problem is solved with the aid of the analog electrical method. It appears that in the whole heat-sinking process occurring in a typical RW laser diode the heat extraction through the ridge plays only a supplementary role, as 60–70% of the heat flux generated in its active area flows through the substrate. The theoretical value of the thermal resistance of the standard ($S = 5$ $\mu$m) ridge-waveguide laser diode is equal to 52 K/W.

## 1. Introduction

The ridge-waveguide configuration of laser diodes provides reliable, low threshold and stable transverse and (sometimes) longitudinal monomode operation characterized by a highly linear light-current curve. These comparatively low-expense lasers are capable of excellent performance at 0.85 $\mu$m [1], [2], 1.3 $\mu$m [3]–[6] and 1.55 $\mu$m [3], [7]–[9]. Only one stage of epitaxial growth on a planar substrate is required followed by a small number of photo-lithographic and etching stages to define the ridge structure.

The simple fabrication process with any of the common epitaxial growth techniques allows the simultaneous realization of both the lateral current and the mode confinement in a single processing step. Thus, an important advantage of the ridge structure is that it avoids the possibility of damage to the active area by the processing steps that provide these confinements. This rather simple laser structure makes a favourable alternative to the numerous types of index-guided laser diodes, first of all to the more complicated buried-heterostructure devices.

A schematic drawing of the (InGa)(AsP)/InP metal-clad ridge-waveguide (MCRW) laser for the wavelength $\lambda = 1.3$ $\mu$m [5], [6] is shown in Fig. 1. The heteroepitaxial layers for these lasers are grown on (100) n-doped ($n = 5 \times 10^{18}$ cm$^{-3}$) InP substrates in a single epitaxial process and contain the following five (or six) layers: i) 3–8 $\mu$m thick n-doped ($n = 5 \times 10^{17}$ cm$^{-3}$) InP buffer layer, ii) 0.14–0.20

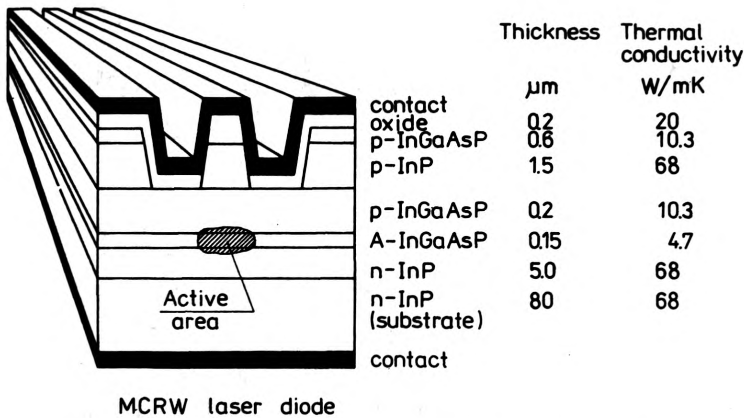


Fig. 1. Schematical drawing of the (InGa)(AsP)/InP metal-clad ridge-waveguide (MCRW) laser

μm thick undoped (InGa)(AsP) active layer ($\lambda = 1.30$ μm), iii) 0.2 μm thick p-doped InP confinement layer (if required [5]), iv) 0.2 μm thick p-doped ($p = 1 \times 10^{17}$ $cm^{-3}$) (InGa)(AsP) etch-stopping layer ($\lambda = 1.02$–$1.05$ μm), v) 1.2–1.5 μm thick p-doped ($p = 5 \times 10^{17}$ $cm^{-3}$) InP ridge layer and vi) 0.2–0.6 μm thick p-doped ($p = 4 \times 10^{18}$ $cm^{-3}$) (InGa)(AsP) cap layer ($\lambda = 1.30$ μm).

The epitaxial growth is followed by a shallow Zn diffusion (10 sec at 600° C [6]); a Zn-doped oxide source being used in order to improve the contact resistance into the cap layer. Thereby the hole concentration in this layer is increased up to $5 \times 10^{19}$ $cm^{-3}$. Then 3–5 μm stripes are defined photolithographically along the [011] direction and the ridges are obtained by ion milling through the cap layer and subsequent selective etching of the InP ridge layer with [5]: HCL : $H_3PO_4$ (1:1) down to the top of the etch-stopping layer.

Electric isolation of the non-lasing area is accomplished by deposition of a 0.2–0.3 μm thick layer of either alumina ($Al_2O_3$), or silicon nitride ($Si_3N_4$), or silicon dioxide ($SiO_2$). The vertical walls of the ridge are (RW lasers [7]–[10]) or are not (MCRW lasers [3]–[6]) coated with the isolating layer. In the previous MCRW GaAs/(AlGa)As laser diodes the lateral current confinement had been achieved by the high contact resistance of the Cr/Au alloy on the low-doped p-type (AlGa)As layer and the excellent contact to the p-type GaAs layer [1], [2], [11], [12]. Therefore these lasers had been completely without oxide layers.

After evaporating a broad area, p-contact (Ti – 40 Å thick, Pt – 500 Å thick and Au – 5000 Å thick layers [13]), thinning the sample, evaporating and alloying the n-contact (Au – 100 Å thick, Sn – 50 Å thick and Au – 5000 Å thick layers [13]), the wafers are cleaved into individual laser chips, usually 200 μm long and 500 μm wide. A double-channel structure [7], [9] is often used in order to facilitate the upside-down mounting of the laser chips.

Waveguiding in the ridge structure of the laser is achieved by the reduction of the effective refractive index in the vicinity of the stripe active area due to the closer spacing between the metal contact and the active layer. By an appropriate choice of the waveguide parameters, MCRW lasers can be realized with a built-in in-

dex-guiding high enough to dominate over the gain-induced guiding mechanism [4], [14], [15]. The dependence of the longitudinal mode spectrum on the construction parameters of MCRW lasers was investigated in [16] and a rigorous waveguide model of these lasers was developed in [17].

Lately information about more complicated ridge laser structures, e.g., double-contacted MCRW lasers [18], [19], brigde-contacted ridge-waveguide (BCRW) lasers [20], MCRW distributed feedback lasers [21] and ridge single-quantum-well graded-index separate confinement heterostructure (SQW GRIN–SCH) lasers [22], have been also published.

The MCRW and the RW (InGa)(AsP)/InP laser diodes seem to be of the most promising coherent light sources for fibre-optical communication. On the other hand, thermal resistance and the associated design for the optimum performance of (InGa)(AsP)/InP laser diodes in a continuous and rapidly pulsed operation is significant, because of their distinctly temperature-dependent operation characteristics (see, e.g., [23]–[29]). Therefore, it seemed worthwhile to investigate the thermal properties of these lasers.

In the present work, the thermal model of the 1.3-$\mu$m MCRW (InGa)(AsP)/InP laser diodes is formulated and their thermal properties are examined both theoretically and experimentally. The work is organized as follows: the theoretical model is presented in this part; experimental results and the influence of various construction parameters on thermal properties of the lasers are discussed in the second part. Some preliminary results of the work were published elsewhere [30].

## 2. Hitherto existing models

The thermal resistance of a laser diode has a significant effect on its operation characteristics. Therefore the reduction of this resistance is a key agent in improving the cw-performance of a laser diode.

In the case of the MCRW laser diode, the first attempt of this kind was made by Stegmueller et al. [31]. They reduced the thermal resistance of the p-side-up mounted laser diodes by a heat spreader, formed by the galvanically strengthened Au-top contact. The heat spreader caused equalization of the temperature distribution in the active region which drops the maximum temperature within itself.

A low thermal resistance of laser diodes can be realized by mounting the diode with the junction down (p-side-down configuration) on the heat sink to minimize the distance between the main heat source and the heat sink [32], [33]. This structure is analysed in the present work. This configuration, however, owing to the nonplanar surface of ridge-waveguide lasers, is rather complicated and, in order to get a quasi-planar surface on the laser chips, a double-channel structure [7], [9] is usually applied. This structure compared to the planar one exhibits an enhanced thermal resistance.

A simplified analysis of thermal resistances for such quasi-planar ridge-waveguide lasers was performed by Amann [34]. Assuming an isothermal active region, he obtained (by means of conformal mapping) approximate analytical expressions for

the averaged thermal resistance. But some of his numerous assumptions seem to be unjustified, e.g., he disregards of the temperature increase in the contact layers and in the heat sink, assumed thermally isolated channel regions, and considered the layered laser structure as being uniform area. Nevertheless, he was right in pointing out that in a typical MCRW laser diode the heat dissipation was connected mainly with the heat path to the heat sink in the regions beyond the ridge. The advantage of his simplified model is its easy applicability to practical devices with a reasonable accuracy. Due to its analytical formulation, the model is clear to everyone and can be easily adapted to new geometries or new devices.

Recently the heat spreading in the RW laser has been analysed numerically by PIPREK and NUERNBERG [35]. They have, however, neglected the thermal resistance of the contact layers, spreading thermal resistance of the heat sink and the radiative transfer of spontaneous energy. Nevertheless, they have determined two-dimensional temperature distributions perpendicular to the ridge and have presented them in terms of isotherm plots.

## 3. Assumptions

The analysis of heat-flux spreading in the ridge-waveguide laser is rather complex because of its "ridge" construction, multilayer structure and non-homogeneous boundary conditions. The last feature is due to the fact that the most part of the upper surface of the laser is covered with an oxide layer, the thermal conductivity of which is relatively low. The vertical walls of the ridge are or are not covered with the isolating layer, from now on, called for simplicity the oxide layer.

It is rather impossible to find an exact analytical solution of this heat spreading problem. Numerical methods, in turn, are much time-consuming and need a very quick and powerful computer. Therefore the problem is solved in this work by means of the analog electrical model. An active area is divided into $2N+1$ identical segments

$$(2N+1)\Delta y = S \qquad (1)$$

where $S$ is the stripe width and $\Delta y$ is the segment width. Spread of the current (i.e., the heat flux) generated in each segment is considered separately. The spreading phenomenon is described properly if a sufficiently high value of $N$ is assumed (in this work $N = 100$). A resultant potential (i.e., temperature) distribution is obtained using the superposition rule.

Assumptions of the model are as follows:

1. We neglect the current-spreading effect because of the negligible thickness of the p-type etch-stopping (InGa)(AsP) layer (this effect can be easily taken into account in the analog electrical model assuming different outputs of the current generation in individual segments of the active layer).

2. We neglect heat-fluxes in lateral directions in the second (active), the third (if exists) and the forth (etch-stopping) layers, because of their negligible thicknesses, i.e., we assume that heat flux flows through these thin layers only perpendicularly.

3. We neglect the temperature dependence of the thermal conductivity because of small temperature increases involved (ridge-waveguide lasers exhibit low-threshold operation).

4. We consider only the most efficient heat source which exists in the active region because: (i) the Joule generation in all layers is negligible in these low-threshold devices, and (ii) the absorption of the spontaneous radiation transferred through the wide-gap layers [36] takes place either very close to the heat sink (in the p-type cap (InGa)(AsP) layer) or very far from it (at the n-side-contact/substrate interface, from where this heat flux is conducted to a considerable extent by a metallization layer and a bonding wire) and resulting heat output is at least one order of magnitude lower than the above main head source (see, e.g., [37] for the GaAs/(AlGa)As lasers where the efficiency of this transfer is similar).

Table 1. Thermal conductivities of the layers of the MCRW laser diodes

| Material | Notation | Value [W/mK] | Ref. |
|---|---|---|---|
| InP | $k_s$ | 68 | [42] |
| $Ga_{0.28}In_{0.72}As_{0.62}P_{0.38}$ | $k_n$ | 5.5 | [43], [44] |
| $Ga_{0.09}In_{0.91}As_{0.20}P_{0.80}$ | $k_w$ | 9.6 | [43], [44] |
| oxide, $SiO_2$ | $k_o$ | 1 | [45] |
| contact layers: | | | |
| Ti | $k_{c,1}$ | 22 | [46] |
| Pt | $k_{c,2}$ | 73 | [46] |
| Au | $k_{c,3}$ | 318 | [46] |
| In | $k_{c,4}$ | 87 | [46] |
| heat sink, Cu | $k_{HS}$ | 400 | [46] |
| Heat sink, Si | $k_{HS}$ | 135 | [47] |

In the calculations, the multilayer structure of the laser, as well as the thermal resistance of contact and oxide layers and the spreading thermal resistance of the heat sink are taken into account. All thermal conductivities are listed in Table 1. The nominal set of the parameters and the notation used in the calculations are presented in Table 2.

The heat generation in the active area is mainly connected with nonradiative recombination within this region and its density may be expressed in the following way [38]:

$$g = \{I_{th}(1-a_{sp}f)+(I-I_{th})[1-a_{ext}-(1-a_i)a_{sp}f]\}U/d_A SL, \ \mathrm{W/m^3} \tag{2}$$

where $U$ is the voltage drop at the p-n junction; $I$ and $I_{th}$ are the supply current and the threshold current, respectively; $a_{sp}$, $a_{ext}$ and $a_i$ are the internal quantum efficiency of the spontaneous emission, the external differential quantum efficiency of the lasing and the internal quantum efficiency of the lasing, respectively, and $d_A$, $S$ and $L$ are dimensions (thickness, width and length, respectively) of the active area.

Coefficient $f$ describes the fraction of the spontaneous emission from the active region, transferred radiatively through the wide-gap layers; it is composed of two parts

$$f = f_n + f_p, \tag{3}$$

Table 2. Nominal set of the parameters used in the calculations for a typical MCRW (InGa)(AsP)/InP laser diode

| Parameter | Notation | Value | Unit |
|---|---|---|---|
| Ambient temperature | $T_A$ | 300 | K |
| Number of sections | $N$ | 100 | – |
| Supply current | $I$ | 100 | mA |
| Threshold current | $I_{th}$ | 25 | mA |
| Voltage drop at the p-n junction | $U$ | 0.95 | V |
| Quantum efficiencies: | | | |
| internal spontaneous | $a_{sp}$ | 50* | % |
| external differential | $a_{ext}$ | 40* | % |
| internal lasing | $a_i$ | 100* | % |
| Transfer coefficient | $f$ | 0.633 | – |
| Chip length | $L$ | 200 | μm |
| Chip width | $W$ | 400 | μm |
| Stripe width | $S$ | 5 | μm |
| Groove width | $C$ | 15 | μm |
| Thicknesses of the layers: | | | |
| n-type InP | $d_n$ | 85 | μm |
| active $Ga_{0.28}In_{0.72}As_{0.62}P_{0.39}$ | $d_A$ | 0.15 | μm |
| p-type InP confinement | $d_{con}$ | 0 | μm |
| etch-stopping $Ga_{0.09}In_{0.91}As_{0.20}P_{0.80}$ | $d_{ES}$ | 0.3 | μm |
| ridge p-type InP | $d_p$ | 1.5 | μm |
| cap $Ga_{0.28}In_{0.72}As_{0.62}P_{0.38}$ | $d_c$ | 0.6 | μm |
| oxide layers: | | | |
| – beyond the ridge | $d_o$ | 0.2* | μm |
| – on vertical walls of the ridge | $d_{ox}$ | 0* | μm |
| contact layers: | | | |
| Ti | $d_{c,1}$ | 40* | Å |
| Pt | $d_{c,2}$ | 500* | Å |
| Au | $d_{c,3}$ | 5000* | Å |
| In | $d_{c,4}$ | 10 | μm |

* Ref. [13]

which may be expressed as follows [39]:

$$f_n = \sin^2(\beta_n/2), \tag{4}$$

$$f_p = \sin^2(\beta_p/2). \tag{5}$$

$\beta_n$ and $\beta_p$ are the respective critical angles at the interfaces of the n-side and p-side heterojunctions confining the active layer, i.e.:

$$\sin\beta_n = n_n/n_A, \tag{6}$$

$$\sin\beta_p = n_p/n_A \tag{7}$$

where $n_A$, $n_n$ and $n_p$ are refractive indices of the active layer and of the n-type and p-type parts of the double-heterostructure, respectively.

## 4. Calculations

In the analog electrical model, spread of the current generated in one segment (say: $i$-th segment) of the active area is schematically shown in Figure 2. The current is divided into two parts: one flowing through the ridge, and the other which flows through the substrate. The latter, in turn, is composed of leftwards and rightwards parts. For these current paths, the corresponding thermal resistances are denoted by $R_A(i)$, $R_{B,L}(i)$ and $R_{B,R}(i)$, respectively. They form a simple current circuit shown in Fig. 3.

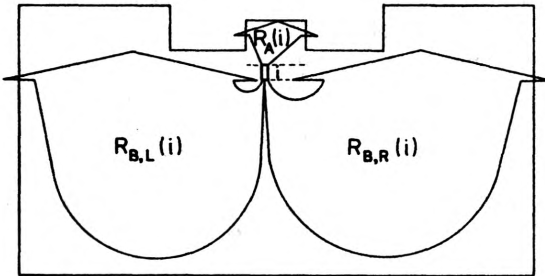


Fig. 2. Spreading of the current generated in the $i$-th segment of the active area in the analog electrical model of the ridge-waveguide laser

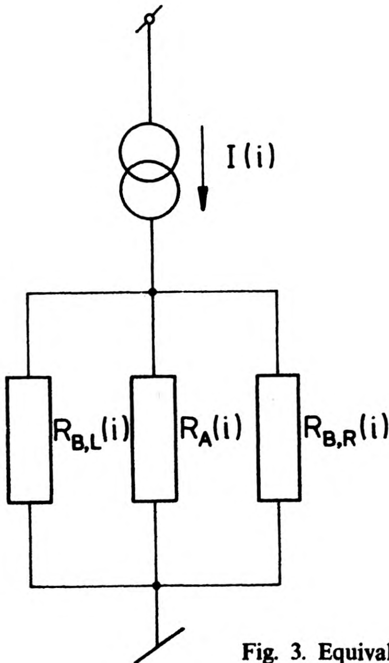


Fig. 3. Equivalent electrical circuit of the current spreading shown in Fig. 2

### 4.1. Calculations of the $R_B$ thermal resistance

The current (i.e., the heat flux) generated in the $i$-th segment may by calculated as follows:

$$I = Q = gd_A L\Delta y \tag{8}$$

where $g$ is given by Eq. (2). In the model in which a current-spreading effect is considered $g$ is position-dependent.

The leftward part of the heat spread through the substrate, for the heat flux generated in the $i$-th segment of the active area, is schematically shown in Fig. 4. The shapes of individual heat paths assumed with the aid of the Kirchhoff's laws for an electric circuit are based on our knowledge of the real structure of the RW laser. An error which accompanying this simplified assumption seems to be insignificant because of the relatively high number (i.e., 201) of individual heat paths considered in the model. The heat flow from the active layer directly in the $y$ direction, i.e., along the (InGa)(AsP) layers, is neglected because of their small thicknesses and low thermal conductivities ($k_n = 5.5$ W/mK for the active layer and $k_w = 9.6$ W/mK for the etch-stopping layer) as compared with the InP layers ($k_s = 68$ W/mK). Hence, it is assumed that heat flows perpendicularly through all these low-thermal-conductivity (InGa)(AsP) layers.

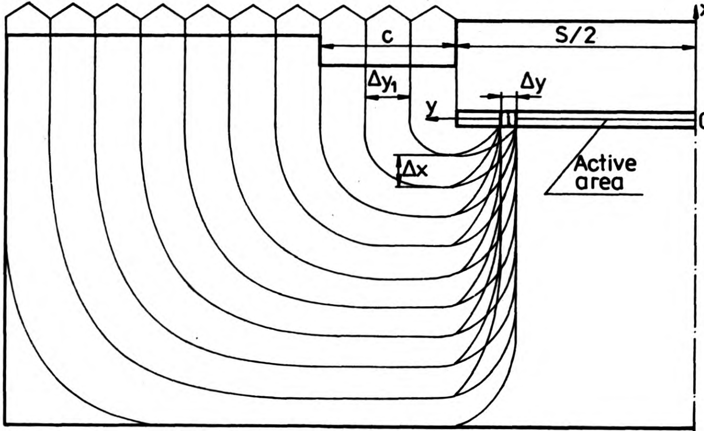


Fig. 4. Leftward part of the spreading through the substrate of the heat generated in the $i$-th segment of the active area. $S$ and $C$ are the widths of stripe and the groove, respectively, and $\Delta y$ is the width of the active area segment. The coordinate system is also shown

An analog electrical circuit, corresponding to the above heat spreading model, is shown in Fig. 5. The composite resistances are as follows:

$$R_{L1} = R_1\mu, \tag{9}$$

$$R_{L2}(i,j) = [\pi/(2Lk_s)]\Pi(y(i), x(j), \Delta y, \Delta x), \tag{10}$$

$$R_{L3}(j) = [\pi/(2Lk_s)]\Pi(x(j), b(j), \Delta x, \Delta y_1), \tag{11}$$

$$R_{L4}(j) = R_s(j) + R_{c,B} + R_{o,B} + R_{HS,B}. \tag{12}$$

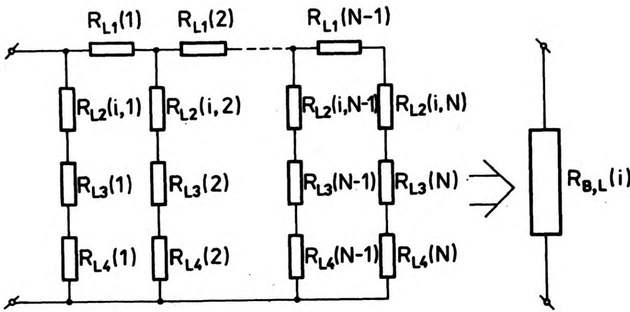


Fig. 5. Analog electrical circuit corresponding to the heat spreading shown in Fig. 4. The notation is explained in the text

The $R_{L1}$ resistance includes the overlapping of heat paths:

$$R_1 = \Delta x/(\Delta y L k_s) = (2d_s)/(SLk_s), \tag{13}$$

$$\mu = \Delta y/(2S). \tag{14}$$

In the calculations of the $R_{L2}$ and $R_{L3}$ resistances we have used the formula (C2) derived in the Appendix C

$$\Pi(a,b,\Delta a,\Delta b) = \frac{1}{\Delta b-\Delta a}\left\{(b-a)+\left[a-\frac{\Delta a(b-a)}{\Delta b-\Delta a}\right]\ln(\Delta a/\Delta b)\right\}, \tag{15}$$

with:

$$b(j) = (j-0.5)\Delta y_1, \tag{16}$$

$$x(j) = (j-0.5)\Delta x, \tag{17}$$

$$y(i) = (N-i+0.5)\Delta y, \tag{18}$$

$$\Delta y_1 = \Delta y(W/S-1). \tag{19}$$

In the above relations, $k_s$ is the thermal conductivity of InP and $d_n$ is the thickness of the n-type InP layer (the substrate layer plus the buffer layer)

$$d_n = N\Delta x. \tag{20}$$

The $R_{L4}$ resistance is calculated for the one-dimensional heat flow, where the thermal resistances for the semiconductor layers ($R_s$), for the contact layers ($R_{c,B}$), for the oxide layer ($R_{o,B}$) and the equivalent thermal resistance [40] of the heat sink ($R_{HS,B}$) may be expressed as follows:

$$R_s(j) = \{d_A/k_n + d_{ES}/k_w + K[(d_p/k_s)+(d_c/k_n)]\}/(L\Delta y_1), \tag{21}$$

$$R_{c,B} = \sum_n (d_{c,n}/k_{c,n})/(L\Delta y_1), \tag{22}$$

$$R_{o,B} = d_o/(L\Delta y_1 k_o), \tag{23}$$

$$R_{HS,B} = [(W-S)/(2\pi\Delta y_1 k_{HS}L)\{\mathrm{arsh}(B)+B\,\mathrm{arsh}(1/B) - (1/3)[(1/B)(B^2+1)^{3/2}-1/B-B^2]\} \quad (24)$$

where: $d_{ES}$, $d_p$ $d_c$, $d_{c,n}$ and $d_o$ are thicknesses of the p-doped (InGa)(AsP) etch-stopping layer, the p-doped InP ridge layer, the p-doped (InGa)(AsP) cap layer, the $n$-th layer of the contact (see Tab. 2), and the oxide layer, respectively, $B = 2L/(W-S)$, all $k$ are thermal conductivities listed in Tab. 1, and the $K$ coefficient is given by:

$$K = \begin{cases} 1 & \text{for } j>j_c, \\ 0 & \text{for } j\leqslant j_c \end{cases} \quad (25)$$

with $j_c = C/\Delta y_1$, where $C$ is the width of the channels.

For the typical construction of the MCRW (InGa)(AsP)/InP laser diode (see Tab. 2), the calculated averaged values of the $R_{B,L}$ and $R_{B,R}$ thermal resistances are equal to 173 K/W.

### 4.2. Calculations of the $R_A$ thermal resistance

For each $i$-th segment of the active area, the thermal resistance $R_A(i)$ is composed of three, parallelly connected parts $R_{A1}$, $R_{A2}$ and $R_{A3}$ (see Fig. 6)

$$1/R_A(i) = 1/R_{A1}(i)+1/R_{A2}(i)+1/R_{A3}(i). \quad (26)$$

We neglect the refraction of the heat fluxes on the InP/(InGa)(AsP) heteroboundary, on the basis of our earlier calculations [41], as well as the possible curving of heat paths within the ridge, because of relatively small thicknesses of both the p-type ridge InP and the cap (InGa)(AsP) layers. Assuming that the thermal conductivity of the heat sink material is much higer than thermal conductivities of the oxide and the semiconductor layers (see Tab. 1), and making use of the formulas (B13) and (B14) derived in the Appendix B, we may calculate these resistances in the following way:

$$R_{A1}(i) = hJ_R(p_{1A1},p_{2A})/(k_s\Delta yL)+R_{c,A1}+eR_{o,A1}+R_{HS,A1}, \quad (27)$$

$$R_{A2}(i)+R_{s,A}(i)+R_{c,A2}+R_{HS,A2}, \quad (28)$$

$$R_{A3}(i) = hJ_R(p_{1A3},p_{2A})/(k_s\Delta yL)+R_{c,A3}+eR_{o,A3}+R_{HS,A3}, \quad (29)$$

with:

$$J_R(p_1,p_2) = [(\pi/2)(p_1^2p_2+1/p_1)+\ln|p_1^2p_2|(p_1p_2-1)]/[p_1^{-2}+(p_1p_2)^2], \quad (30)$$

$$h = d_{ES}k_s/k_w, \quad (31)$$

$$H = d_p+d_ck_s/k_n, \quad (32)$$

$$p_{1A1} = \Delta y(i-0.5)/h, \quad (33)$$

$$p_{1A3} = \Delta y(2N-i+0.5)/h, \quad (34)$$

$$p_{2A} = H/\Delta y. \quad (35)$$

The thermal resistances for the contact layers ($R_c$), the oxide layer ($R_o$) and the equivalent thermal resistances [36] of the heat sink ($R_{HS}$) are given by:

$$R_{c,A1} = R_{c,A3} = \sum_n (d_{c,n}/k_{c,n})/[(d_p+d_c)L], \tag{36}$$

$$R_{c,A2} = \sum_n (d_{c,n}/k_{c,n})/(SL), \tag{37}$$

$$R_{o,A1} = R_{o,A3} = d_o/[(d_p + d_c)Lk_o], \tag{38}$$

$$R_{HS,A1} = R_{HS,A3} = \{0.5+\ln[2L/(d_p+d_c)]\}/(\pi L k_{HS}), \tag{39}$$

$$R_{HS,A2} = [0.5+\ln(2L/S)]/[\pi(L/S)\Delta y k_{HS}], \tag{40}$$

$$R_{s,A}(i) = \left\{\sum_{j=1}^{2N}[1/R(i,j)]\right\}^{-1}, \tag{41}$$

with

$$R(i,j) = \{[(h+H)^2+\Delta y^2(i-j)^2]^{1/2}\}/(\Delta y L k_s), \tag{42}$$

$$e = \begin{cases} 1 \text{ for vertical walls coated with the oxide layer,} \\ 0 \text{ for vertical walls not coated with the oxide layer.} \end{cases} \tag{43}$$

For the nominal set of the parameters listed in Tab. 2, the calculated averaged value of the $R_A$ thermal resistance is equal to 133 K/W.

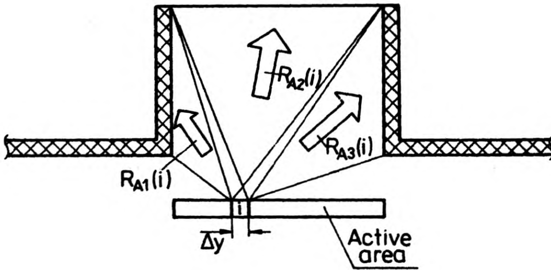


Fig. 6. Spreading (through the ridge) of the current generated in the *i*-th segment of the active area in the analog electrical model. $R_{A1}$, $R_{A2}$ and $R_{A3}$ are composite thermal resistances. The vertical walls of the ridge are or are not coated with the oxide layer (both cases are considered in the calculations)

## 5. Conclusions

In this work, the theoretical model of heat-flux spreading in a ridge-waveguide laser was presented. To this end we have used the analog electrical method.

The active area was divided into $2N+1$ identical segments and the heat spreading was considered for each segment separately. The resultant temperature distribution was obtained with the aid of the superposition rule.

The heat flux generated in each segment of the active area was divided into two parts: one flowing through the ridge and the other through the substrate. The corresponding thermal resistances were calculated separately in the model. Their values are in a close agreement with the experimental results.

The calculated averaged values of the composite thermal resistances $R_A = 133$ K/W and $R_{B,L} = R_{B,R} = 173$ K/W (see Fig. 3) give the total thermal resistance of the typical MCRW laser diode (Tab. 2) equal to 52 K/W. From the above values it appears that in a RW laser the heat extraction through the ridge plays only supplementary role in the whole heat-sinking process, and that 60–70% of the heat flux generated in its active area flows through the substrate. This conclusion is in agreement with the results of earlier theoretical papers, i.e., [34] and [35].

In the second part [48] of the work, the experimental results are presented and compared with the theoretical ones and the influence of various construction parameters on thermal properties of a ridge-waveguide laser is discussed.

# Appendix A

## Determination of the thermal resistance for a heat flow between skew faces of a trapezoid prism

Let us derive a formula for the thermal resistance in the case of a heat flow between skew faces of a trapezoid prism (notation used in the calculations is explained in Fig. A). The height of the trapezoid is then equal to

$$P_{t,0} = \Delta y X/(X^2 + Y^2)^{1/2} = \text{const.} \tag{A1}$$

A width of a heat flux flowing through the trapezoid is a function of position

$$P_t(\gamma) = R(\gamma)\Delta y/Y. \tag{A2}$$

Therefore, the increment of the thermal resistance may be written as

$$dR_t(\gamma) = R(\gamma)d\gamma/(kP_t(\gamma)L) = Yd\gamma/(k\Delta yL) \tag{A3}$$

where $L$ is a height of the prism (see Fig. A), and $k$ is the thermal conductivity of a prism meterial.

After integration, we get finally the following formula for the thermal resistance:

$$R_t = \int_0^{\pi/2} dR_t(\gamma) = \pi Y/(2k\Delta yL). \tag{A4}$$

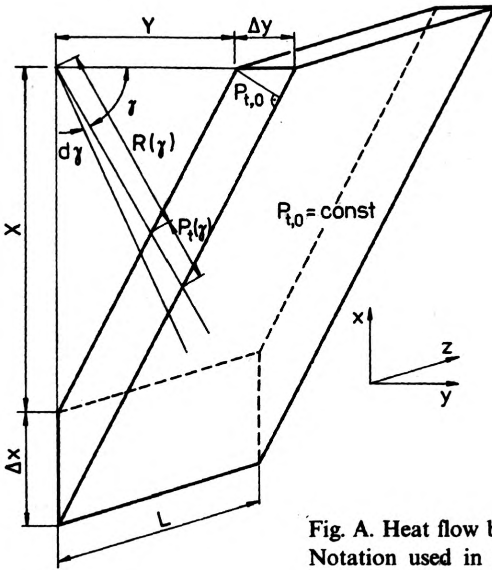


Fig. A. Heat flow between skew faces of a trapezoid ($P_{t,0}$ = const) prism. Notation used in the calculations is shown

# Appendix B

## Determination of the thermal resistance for a heat flow between skew faces of a generalized trapezoid prism

Let us consider a heat flow between skew faces of a generalized trapezoid prism shown in Fig. B, which includes the explanation of notation used in the calculations. In this case, the height of the generalized trapezoid is not constant, changing from

$$P_{G,0}(\gamma = 0) = \Delta y X/(X^2+Y^2)^{1/2} \quad \text{for } \gamma = 0, \tag{B1}$$

to

$$P_{G,0}(\gamma = \pi/2) = \Delta x Y/(X^2+Y^2)^{1/2} \quad \text{for } \gamma = \pi/2. \tag{B2}$$

Let us introduce two parameters:

$$p_1 = Y/X, \tag{B3}$$

$$p_2 = \Delta x/\Delta y. \tag{B4}$$

Then the height of the generalized trapezoid may be written as

$$P_{G,0}(\gamma) = \Delta y[X+(p_2 Y - X)x'/X] \neq \text{const}. \tag{B5}$$

Following the approach used in the Appendix A, we now find the width of a heat flux flowing through the trapezoid in the following form:

$$P_G(\gamma) = P_{G,0}(\gamma)R(\gamma)[(X^2+Y^2)^{1/2}]/(XY). \tag{B6}$$

By inserting Equation (B5) and the formula

$$x'/X = [1+(X/Y)\,\mathrm{cotan}\,\gamma]^{-1} \tag{B7}$$

into Eq. (B6), we get

$$P_G(\gamma) = [R(\gamma)\Delta y/(XY)][(X^2\mathrm{cotan}(\gamma)+Y^2p_2)/(X\mathrm{cotan}(\gamma)+Y)]. \tag{B8}$$

Hence the increment of the thermal resistance becomes

$$\begin{aligned} dR_G(\gamma) &= [R(\gamma)\,d\gamma]/[kP_G(\gamma)L] \\ &= [(XYd\gamma)/(k\Delta yL)][(X\mathrm{cotan}(\gamma)+Y)/(X^2\mathrm{cotan}(\gamma)+Y^2p_2)] \\ &= [(Xd\gamma)/(k\Delta yL)]\{[1+p_1\tan(\gamma)]/[p_1^{-1}+p_1p_2\tan(\gamma)]\}. \end{aligned} \tag{B9}$$

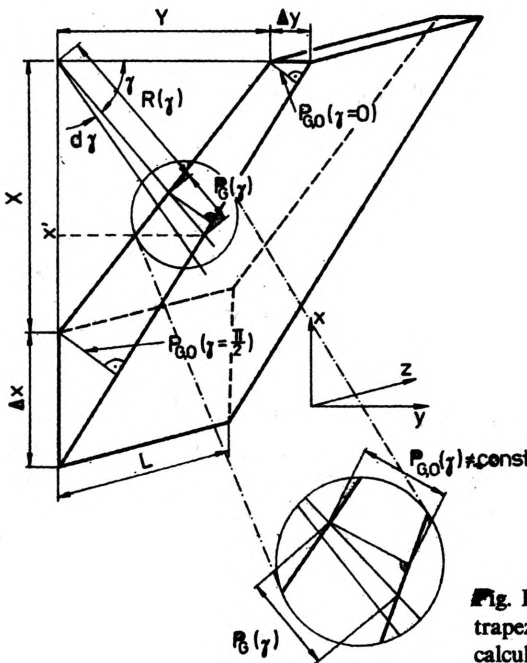


Fig. B. Heat flow between skew faces of a generalized trapezoid ($P_{G,0}$ = const) prism. Notation used in the calculations is shown

The thermal resistance is obtained with the aid of the following integration:

$$R_G = \int_0^{\pi/2} dR_G(\gamma), \tag{B10}$$

so we take advantage of two following integrals [49]:

$$\int dx/(a+b\tan x) = [b\ln|a\cos x+b\sin x|+ax]/(a^2+b^2), \tag{B11}$$

$$\int \tan x\,dx/(a+b\tan x) = [bx-a\ln|a\cos x+b\sin x|\,]/(a^2+b^2). \tag{B12}$$

After integration and some mathematical manipulations, we finally obtain the thermal resistance in the following form:

$$R_G = XJ_R(p_1,p_2)/(k\Delta yL), \tag{B13}$$

with

$$J_R(p_1,p_2) = [(\pi/2)(p_1^2+p_1^{-1})+\ln|p_1^2p_2|(p_1p_2-1)]/[p_1^{-2}+(p_1p_2)^2]. \tag{B14}$$

For the case of the constant height of the trapezoid

$$P_{G,0}(\gamma) = P_{G,0}(\gamma=0) = \Delta yX/[(X^2+Y^2)^{1/2}] = \text{const}, \tag{B15}$$

the above formulas ((B13), (B14)) reduce to the formula (A4).

# Appendix C

## Determination of the thermal resistance for heat flow through a bent trapezoid prism

Let us consider a heat flow through a bent trapezoid prism shown in Fig. C. In this case the increment of the thermal resistance may be written as

$$dR_t(\gamma) = \frac{[a+(b-a)(2\gamma/\pi)]d\gamma}{[\Delta a+(\Delta b-\Delta a)(2\gamma/\pi)]Lk} \tag{C1}$$

where $k$ is the thermal conductivity of the prism material.

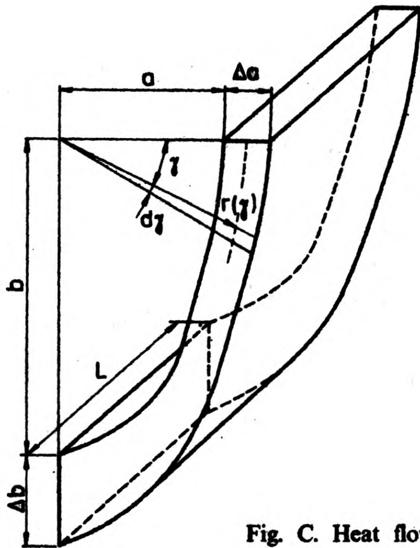


Fig. C. Heat flow through a bent trapezoid prism. Notation used in the calculations is shown

After integration within the limits 0 and $\pi/2$, we finally obtain the thermal resistance $R_t$ of the bent trapezoid prism on the following form:

$$R_t = \frac{\pi}{2Lk(\Delta b-\Delta a)}\left[(b-a)+\left(a-\frac{\Delta a(b-a)}{\Delta b-\Delta a}\right)\ln(\Delta b/\Delta a)\right]. \tag{C2}$$

For $\Delta b = \Delta a$, the above formula reduces to $R_{t,0} = [\pi(b+a)]/(4\Delta aLk)$.

*Acknowledgements* – The authors are indebted to Dr. Markus-Christian Amann, Siemens AG, Research Laboratories, Federal Republic of Germany, for his comments on the manuscript.

The work was partially carried out under the Polish Central Program for Fundamental Research CPBP 01.06., 6.04.

## References

[1] AMANN M.-C., Electron. Lett. **15** (1979), 441–442.
[2] AMANN M.-C., STEGMUELLER B., [In] *Digest of Topical Meeting on Integrated and Guided-Wave Optics*, Optical Society of America, Washington, D. C., 1980, MC3-1.
[3] AMANN M.-C., STEGMUELLER B., BAUMANN C. G., HANKE C., *ECOC'86*, 1986, pp. 85–87.
[4] AMANN M.-C., STEGMUELLER B., *Tenth IEEE International Semiconductor Laser Conference*, Kanazawa, Japan, 1986, paper P4.
[5] AMANN M.-C., STEGMUELLER B., Jpn. J. Appl. Phys., **25** (1986), 228-230.
[6] AMANN M.-C., STEGMUELLER B., Appl. Phys. Lett. **48** (1986), 1027–1029.
[7] KAMINOW I. P., NAHORY R. E., POLLACK M. A., STULZ L. W., DEWINTER J. C., Electron. Lett. **15** (1979), 763–765.
[8] KAMINOW I. P., STULZ L. W., KO J.-S., MILLER B. I., FELDMAN R. D., DEWINTER J. C., POLLACK M. A., Electron. Lett. **19** (1983), 877–879.
[9] ARMISTEAD C. J., WHEELER S. A., PLUMB R. G., MUSK R. W., Electron. Lett. **22** (1986), 1145–1147.
[10] KAMINOW I. P., STULZ L. W., KO J.-S., DENTAI A. G., NAHORY R. E., DEWINTER J. C., HARTMAN R. L., IEEE J., Quantum Electron. **QE-19** (1983), 1312–1319.
[11] AMANN M.-C., Frequenz **34** (1980), 343–346.
[12] AMANN M.-C., STEGMUELLER B., Appl. Opt. **20** (1981), 1483–1486.
[13] AMANN M.-C., private communication.
[14] AMANN M.-C., Archiv für Elektronik und Übertragungstechnik **39** (1985), 311–316.
[15] AMANN M.-C., Archiv für Elektronik und Übertragungstechnik **40** (1986), 185–187.
[16] STEGMUELLER B., Appl. Phys. Lett. **42** (1983), 15–16.
[17] AMANN M.-C., IEEE J. Lightwave Technology **LT-4** (1986), 689–693.
[18] HONSBERG M., Electron. Lett. **20** (1984), 844–846.
[19] HONSBERG M., HARTH W., Int. J. Electronics **60** (1986), 47–50.
[20] HARTL E., MUELLER G., IEE Proceedings **134**, Pt. J. (Optoelectronics), (1987), 22–26.
[21] BAUMANN P. G., Archiv für Elektronik und Übertragungstechnik **40** (1986), 10–14.
[22] HARDER C., BUCHMANN P., MEIER H., Electron. Lett. **22** (1986), 1081–1082.
[23] ASADA M., ADAMS A. R., STUBKJAER K. E., SUEMATSU Y., ITAYA Y., ARAI S., IEEE J. Quantum Electron. **QE-17** (1981), 611–619.
[24] POLLACK M. A., PAWLIK J. R., NAHORY R. E., ANTHONY P. J., IEEE J. Quantum Electron. **QE-17** (1981), 450–453.
[25] YANO M., IMAI H., TAKUSAGAWA M., IEEE J. Quantum Electron. **QE-17** (1981), 1954–1963.
[26] DUTTA N. K., NELSON R. J., IEEE J. Quantum Electron. **QE-18** (1982), 871–878.
[27] DOLGINOV L. M., DURAEV V. P., ELISEEV P. G., NEDELIN E. T., SVERDLOV B. N., SVEIKIN V. I., SHEVCHENKO E. G., Kvantovaya Elektronika **9** (1982), 1902–1904, (in Russian).
[28] NELSON R. J., DUTTA N. K., J. Appl. Phys. **54** (1983), 2923–2929.
[29] ASADA M., SUEMATSU Y., IEEE J. Quantum Electron. **QE-19** (1983), 917–923.

[30] Both W., Nakwaski W., *International Conference on Semiconductor Injection Lasers, SELCO'87*, October 11–16, 1987, Holzhau (GDR), pp. 9–10.
[31] Stegmueller B., Honsberg M., Luy J. F., Harth W., Archiv für Elektronik und Übertragungstechnik **39** (1985), 63–65.
[32] Duda E., Carballes J.-C., Apruzzese J., IEEE J. Quantum Electron. **QE-15** (1979), 812–817.
[33] Nakwaski W., Scientific Bulletin of Łódź Technical University **469** (Physics – 8), (1985), 15–32.
[34] Amann M.-C., Appl. Phys. Lett. **50** (1987), 4–6.
[35] Piprek J., Nuernberg R., *International Conference on Semiconductor Injection Lasers, SELCO'87*, October 11–16, 1987, Holzhau (GDR), pp. 49–50.
[36] Joyce W. B., Dixon R. W., J. Appl. Phys. **46** (1975), 855–862.
[37] Nakwaski W., IEE Proceedings **131** Pt. I (Solid-State and Electron Devices), (1984), 94–102.
[38] Kobayashi T., Furukawa Y., Jpn. J. Appl. Phys. **14** (1975), 1981–1986.
[39] Nakwaski W., Sov. J. Quantum Electron. **9** (1979), 1544–1546; Kvantovaya Elektronika **6** (1979), 2609–2612.
[40] Carslaw H. S., Jaeger J. C., *Conduction of Heat in Solids*, Clarendon Press, Oxford 1959, p. 265.
[41] Nakwaski W., Electron. Lett. **19** (1983), 368–370.
[42] Kudman I., Steigmeier E. F., Phys. Rev. **133** (1964), A1665–A1667.
[43] Nakwaski W., *International Conference on Semiconductor Injection Lasers, SELCO'87*, October 11–16, 1987, Holzhau (GDR), p. 44.
[44] Nakwaski W., J. Appl. Phys. **64** (1988), 159–166.
[45] Bergh A. A., Dean P. J., *Light-Emitting Diodes*, Clarendon Press, Oxford 1976, Table 6.3.
[46] *American Institute of Physics Handbook*, [Ed.] D. E. Gray, McGraw-Hill, New York 1972, Table 4g–8.
[47] Touloukian Y. S., Buyco E. H., *Thermophysical Properties of Matter*, IFI/Plenum, New York 1970, Vol. 5.
[48] Nakwaski W., Both W., Opt. Appl. **20** (1990), 143–164.
[49] Gradshteyn I. S., Ryzhik I. W., *Table of Integrals, Series and Products*, Academic Press, New York 1965, Integrals 2.557.3 and 2.564.3.

*Received September 15, 1989*

## Тепловые свойства лазеров с Н-образным волноводом, прикрепляемых к корпусу стороной p. I. Теоретическая модель

В настоящей работе представлена тепловая модель лазеров с Н-образным волноводом (лазеров RW), прикрепляемых к корпусу стороной p. В модели учтены: многоуровневая структура лазера, тепловое сопротивление контактов и корпуса, а также лучистый трансфер спонтанного излучения. Распространение тепла в анализируемой сруктуре решили, пользуясь подобием тепловых и электрических явлений. Как оказалось, в анализируемых типичных лазерах RW теплоотвод через гребешок играет лишь дополнительную роль во всем процессе теплоотвода. 60–70% потока тепла, генерируемого в их активных областях, проходит через основу. Теоретическое значение теплового сопротивления стандартного лазера RW ($S = 5$ m) составляет 52 K/W.